A Comparison of Topology Optimization Methods for the Design of a Cantilever Beam

A senior thesis submitted to the Carthage College Physics & Astronomy Department in partial fulfillment of the requirements for the Bachelor of Arts Degree in Physics

by

Thomas P. Shannon

Abstract Topology Optimization (TO) is an alternative approach to designing structural parts that produce highly efficient designs by catering to a particular set of initial constraints. This approach to design effectively reduces material waste and provides for lighter structures by creating designs composed of unique geometries that perform similarly to the designs created by humans — but at a fraction of the volume and mass. There are many different TO methods that can accomplish this, however, with TO being recently developed within the past few decades, there is still some debate to which TO method produces the best results. This paper explores two common TO methods: the solid isotropic with material penalization (SIMP) method and the bi-directional evolutionary structure optimization (BESO) method. Each method shall be utilized to design a cantilever beam at several target volumes — a constraint common in TO methods, in which limits the amount of material used within a specific volumetric design space. The structures from each respective TO method shall then be compared through use of static load testing to determine where each structure encounters the highest amount of stress, strain, and displacement. Each structure shall then be tested to its limit by applying increasing amount of mass to determine it's Euler critical load. Using these metrics, it has been found that the BESO method may be more effective for cantilever designs at volume fractions *below* 35%, whereas the SIMP method may be better for designs at volume fractions *above* 35%.

Undergraduate Thesis
Bachelor of Arts, Physics
Advisor: Dr. Brant Carlson
May 5th, 2019

Acknowledgements

This thesis wouldn't have been possible without the extensive support of the Physics and Computer Science departments. I would like to thank Dr. Quashnock for leading the Senior Seminar. It was a long and arduous process, but you were always there to help us along the way. I would also like to thank Dr. Carlson for always being a mentor, helping me through this thesis and many projects, such as RockSat-X. You have always had your door open and always had an answer to almost anything. I would like to thank Dr. Crosby for giving me the opportunities I would have never imagined. The projects with the Wisconsin Space Grant Consortium I have done over the years have greatly shaped the person I am today and I am greatly indebted.

Along with the Physics department, I would like to thank Professor Perry Kivolowitz and Professor Schroeder from the Computer Science department for their aide in the initial development of the software used to generate the designs for the bi-directional evolutionary structure optimization (BESO) method. They made sure I stayed on track of my development and helped make this thesis a reality.

Lastly, I would like to thank my friends and family for always supporting me. There were many points in my college career when I probably took on too much than I should have, which caused for many moments of stress. However, my friends and family were always there for me at every single step — I couldn't have done it without them. So without further adieu: I present to you an accumulation of a year's hard work — my senior thesis.

Contents

1 Introduction **6**

1.1 Stress and Strain 8

1.2 Finite Element Analysis 9

2 Topology Optimization **13**

2.1 Overview of Topology Optimization 13

2.2 Solid Isotropic with Material Penalization (SIMP) 14

2.3 Bi-directional Evolutionary Structure Optimization (BESO) 16

3 Computational & Analytic Results **17**

3.1 Validation of Finite Element Analysis 17

3.2 Topology Optimization Results 19

3.2.1 SIMP Method Optimization Results 20

3.2.2 BESO Method Optimization Results 21

3.2.3 3D Voxel Renderings of SIMP vs. BESO 22

3.2.4 Qualitative Discussion of BESO vs. SIMP Results 23

3.3 Static Load Analysis of SIMP vs. BESO 23

3.3.1 Von Mises Stress and Strain Analysis 25

3.3.2 Displacement Analysis 27

3.3.3 Euler Critical Load Analysis 28

4 Conclusion **31**

4.1 Discussion 31

4.1.1 Finite Element Analysis 31

4.1.2 Optimization Processes 31

4.1.3 Static Load Analysis 32

4.2 Future Research 32

4.3 Ending Notes 33

References **33**

A Finite Element Analysis Lagrange Interpolation **36**

A.1 Shape Functions 36

B Poisson Surface Reconstructed Structures **37**

List of Figures

1.1 AutoDesk moon lander for NASA mission 7
1.2 Surface forces: pressure, tension, shear 8
1.3 Eight nodal coordinate system of hexahedral element 10

2.1 Two dimensional slice of filter radius 14

3.1 Cantilever beam validation test setup 17
3.2 Validation test scenario: FEA Setup 18
3.3 Y-displacement comparison of analytic solution and FEA solution . . 19
3.4 SIMP Method Optimization Process 20
3.5 BESO Method Optimization Process 21
3.6 Comparison of SIMP and BESO 3D Voxel Renderings 22
3.7 Average Stress and Strain vs. Volume Fraction 25
3.8 Average Displacement for each TO method and volume fraction . . . 28
3.9 Euler Critical Load for each TO method and volume fraction 29

B.1 15% VF BESO Cantilever with PSR Filter 37
B.2 15% VF SIMP Cantilever with PSR Filter 38
B.3 25% VF BESO Cantilever with PSR Filter 39
B.4 25% VF SIMP Cantilever with PSR Filter 40
B.5 35% VF BESO Cantilever with PSR Filter 41
B.6 35% VF SIMP Cantilever with PSR Filter 42
B.7 45% VF BESO Cantilever with PSR Filter 43
B.8 45% VF SIMP Cantilever with PSR Filter 44
B.9 55% VF BESO Cantilever with PSR Filter 45
B.10 55% VF SIMP Cantilever with PSR Filter 46

1

Introduction

For millenia, we as humans have created things — from the simple arrow that helped us hunt our food, to the boats that carried us across seas, and now the spacecraft that will carry us to space. We as humans have come a long way and we are always looking to improve the things we create. Traditionally, the method in which we create things has been pretty similar for the past few centuries — we come up with an idea, we design it, and test it in some way.[1] This process is outdated and often times, things could have been designed better. So how can we improve upon this process? Is there a way to use software to ultimately help us create the *"most optimal"* solution for a design that relies on a certain set of criterion?

The answer is yes. There is an emerging technique, known as topology optimization (TO), which does exactly that. TO methods essentially allow us to take a certain set of criterion, such as: a target volume, boundary constraints, and load information to ultimately create the most *"optimal"* design for a part. Using the criterion, TO methods can redistribute a design's material layout in order to conform to the requirements specified by the engineer, while enhancing certain aspects of the design, such as structural stiffness. (Xia, 2018b). TO is still a rather new concept, with most development taking place in the past few decades. However, with new manufacturing techniques, such as 3D printing, many engineers are ditching the *"traditional"* way of design and moving to TO methods in order to produce highly efficient designs that are lighter and will perhaps be cheaper to produce in the future. TO methodology has been proven to be especially important in the aerospace industry, as it costs anywhere from $5,000.00-10,000.00 to send one pound up into

[1] There has been improvements with the emergence of CAD software, but it is relatively a similar process — you come up with an idea, model it, simulate and test, and repeat the process until the design meets the constraints.

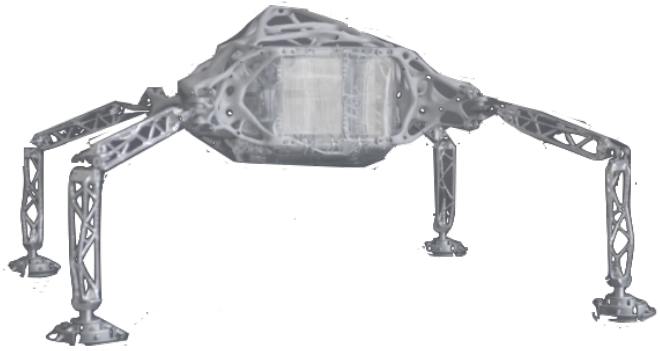

Figure 1.1: **AutoDesk moon lander for NASA mission (Leonard, 2018).** The organic cells cut from the moon lander provide a 30% mass reduction in comparison to old moon lander designs, which would never had been possible through human design.

space. AutoDesk has recently taken an initiative to build software for this technique in order to produce the most economical parts for the aerospace industry.[2] Seen in Figure 1.1, one can see a moon lander design generated by AutoDesk's software. You may notice that the structure is organic-like. These organic-like cells that are cut from structure have effectively allowed AutoDesk to reduce the mass of the traditional moon-lander by approximately 30%. This lead to a massive cost reduction into sending this piece into space.

There are several different methods in TO in which could have helped accomplished a structure like Figure 1.1, and therefore it is important to study how different TO methods compare to one another in order find the *"best"* solution. This paper explores a comparative analysis between the resulting cantilever designs from two different finite-element analysis based TO methods: the solid isotropic with material penalization (SIMP) method and the bi-directional evolutionary structure optimization (BESO) method. Each method will be utilized in order to generate a design for a cantilever beam at several different volume fractions. The paper shall then highlight which method produces a more *"effective"* cantilever beam structure by conducting static load scenarios using driving parameters such as structure displacement, stress, strain, and Euler critical load. With this information, we can ultimately use physics in order to help aide us in understanding how each TO method performs. In the following subsections, a background in stress, strain, and finite element analysis will be given to help the reader better understand the results in following sections.

[2] AutoDesk more realistically uses what is known as *"generative adversarial networks"* — a form of neural network that is fueled on topology optimization data.

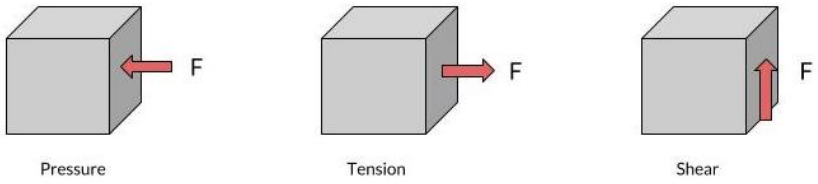

Figure 1.2: **Surface forces: pressure, tension, shear.** There are three different surface forces in which include: pressure, tension, and shear. Pressure acts normally inward to the surface, tension acts normally outward to the surface, and shear acts tangentially upon the surface.

1.1 Stress and Strain

In order to better understand the underlying physics of these structures, a background in material stress and strain is needed. In typical statics problems a structure is often analyzed when a load is set upon it in a particular location. These loads act upon the surface of the structure and are otherwise known as *surface forces*. These surface forces are distributed over a given area of the structure and produce what is known as *stress*. There are three different surfaces forces that cause stress, which include: pressure, tension, and shear. These are illustrated in Figure 1.2. The relationship between surface forces and area can be expressed by Equation 1.1 to give us the equation of stress, denoted by σ, where $F_{surface}$ is the force acting on the surface and A is the area of that surface.

$$\sigma = \frac{F_{surface}}{A} \tag{1.1}$$

As surface forces act upon the structure, they cause deformations that lead to the structure either stretching or compressing in a particular direction. In order to quantify these deformations we look at the fractional change in the dimensions of the structure, otherwise known as strain, denoted by ϵ. For three-dimensional systems, we typically look at the overall change in the volumetric dimensions of the body or structure. Equation 1.2 represents this relationship, where ΔV is the change in volume of the body and V is the volume of the body. (Taylor, 2005).

$$\epsilon = \frac{\Delta V}{V} \tag{1.2}$$

The relationship between stress and strain represents a form of Hooke's Law, where ϵ represents the displacement and σ represents the restoring force over an area of material. This is represented below in Equation 1.3, which describes how the ratio between stress and strain form what is known as the elastic modulus — the measure of the ability of a material to withstand changes in dimensions when put under stress. The elastic modulus is known by different names based on which type of surface force is acting on the system: young's modulus for tensile stress, bulk modulus for compression stress, and shear modulus for shear stress.

$$E = \frac{\sigma}{\epsilon} \tag{1.3}$$

In statics problems we also look at the strain energy density, the amount of work per unit volume in which the structure does in resistance to the load set upon it. This takes on a very similar form to the potential energy of a spring, as seen in Equation 1.4 and is calculated by TO methods in order to quantify the deformations in either an element or the total structure. This ultimately is used to drive the TO method's process of removing material from the design. This is extremely crucial, as it helps determine where to redistribute material on the structure in order to maximize stiffness - the measure of resistance to deformations caused by surface forces.

$$\psi(\epsilon) = \frac{1}{2} E \epsilon^2 \tag{1.4}$$

1.2 Finite Element Analysis

Pivoting from the information given for stress and strain, we can now use these metrics to determine how a structure performs. In order to determine these metrics, we need to solve the system using what is known as finite element analysis (FEA). FEA is a way of representing a system with infinitesimal elements. Each TO method that is compared in this paper utilizes a grid system composed of what are known as eight-node hexahedral elements (H8). An H8 element is illustrated in Figure 1.3. Each node within the H8 element is able to move in the *alpha*, *beta*, and *gamma* direction, giving each H8 element a total of twenty-four degrees of freedom. When a load is placed on the structure, these nodes are displaced, causing the system to deform. The way we calculate these nodal displacements is done through what is known as, *"the direct stiffness method"*. We will ultimately use these displacements

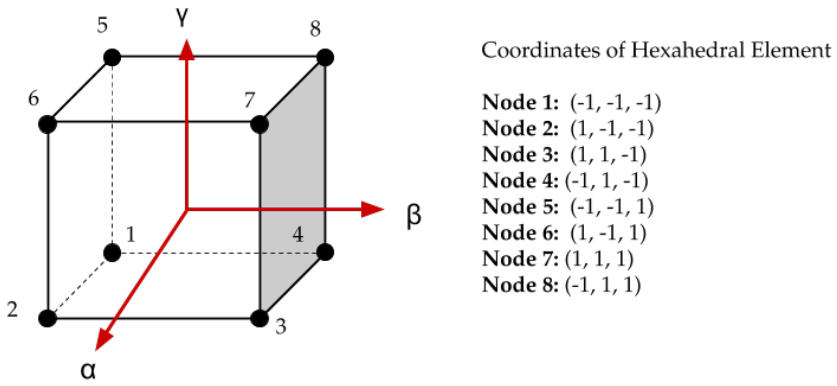

Figure 1.3: **Eight nodal coordinate system of hexahedral element.** Hexahedral elements are composed of six faces and eight nodes connected at each vertices. A common way we represent the state of these nodes is by comparing them to what is known as the *natural coordinate* system — centered at the origin of the element.

later in order to calculate mean compliance, which will help inform the TO material removal process.

The direct stiffness method works on the premise of Equation 1.5, which describes a form of Hooke's Law, where K is the stiffness tensor, u is the displacement tensor, and f is force tensor.

$$Ku = f \tag{1.5}$$

Each TO method in the beginning of it's optimization process specifies a known force at particular locations within the system. These values are then placed in the force tensor in corresponding spots to where they are located in the system, otherwise known as the *"physical coordinate system"*. In order to calculate the displacements, according to Equation 1.5, we also need to formulate the stiffness matrix, which is a system of linear equations that represents how each element resists in response to an applied force. The way we represent the stiffness matrix for a H8 element is given through Equation 1.6, where B_i represents the strain matrix, D represents the elasticity matrix, B_i^T represents the transposed strain matrix, and $\det(J)$ represents the determinant of the Jacobian, which represents mapping between elements in the *"natural coordinate system"*, as described in Figure 1.3, to the physical coordinate system — the coordinate system of the entire system (Liu, 2014)

$$K_e = \int_{-1}^{1}\int_{-1}^{1}\int_{-1}^{1} B_i D B_i^T det(J)\, d\alpha\, d\beta d\gamma \tag{1.6}$$

To further dissect some of the components in Equation 1.6, we can represent these variables through certain approximations. This is typical of most FEA methods and although they do not utilize exact solutions to determine how a structure performs, approximations to how the system acts is sufficient enough for us to generalize different types of scenarios. In order to define the strain matrix of an H8 element, we use what is known as *"Lagrange shape functions"*. Shape functions are functions that help interpolate a solution between each nodal point in the element in the natural coordinate system. The software written for the BESO method in future sections, relies on linear interpolation, as expressed by the functions in Appendix A. By looking at the change of these shape functions with respect to the α, β, and γ directions, we ultimately extrapolate the strain matrix through the approximation as described in Equation 1.7 (Liu, 2014).[3]

$$B_e = \begin{bmatrix} \frac{dN_1}{d\alpha} & 0 & 0 & \dots & \frac{dN_8}{d\alpha} & 0 & 0 \\ 0 & \frac{dN_1}{d\alpha} & 0 & \dots & 0 & \frac{dN_8}{d\alpha} & 0 \\ 0 & 0 & \frac{dN_1}{d\alpha} & \dots & 0 & 0 & \frac{dN_8}{d\alpha} \\ \frac{dN_1}{d\beta} & \frac{dN_1}{d\alpha} & 0 & \dots & \frac{dN_8}{d\beta} & \frac{dN_8}{d\alpha} & 0 \\ 0 & \frac{dN_1}{d\gamma} & \frac{dN_1}{d\beta} & \dots & 0 & \frac{dN_8}{d\gamma} & \frac{dN_8}{d\beta} \\ \frac{dN_1}{d\gamma} & 0 & \frac{dN_1}{d\alpha} & \dots & \frac{dN_8}{d\gamma} & 0 & \frac{dN_8}{d\alpha} \end{bmatrix} \tag{1.7}$$

In order to formulate Equation 1.6, we also need the elasticity matrix, which is defined by the material properties of the system and Poisson's ratio. For an H8 element, this is given by Equation 1.8, where E represents the elastic modulus and ν is Poisson's ratio (Liu, 2014). The Poisson ratio factors account for the ratio of the proportional decrease in a lateral measurement to the proportional increase in length of a particular direction for a material that is elastically stretched.

$$D = \frac{E}{(1+\nu)(1-2\nu)} X \begin{bmatrix} 1-\nu & \nu & 0 & 0 & 0 & 0 \\ \nu & 1-\nu & \nu & 0 & 0 & 0 \\ 0 & \nu & 1-\nu & 0 & 0 & 0 \\ 0 & 0 & 0 & \frac{1-2\nu}{2} & 0 & 0 \\ 0 & 0 & 0 & 0 & \frac{1-2\nu}{2} & 0 \\ 0 & 0 & 0 & 0 & 0 & \frac{1-2\nu}{2} \end{bmatrix} \tag{1.8}$$

[3]These six-dimensional matrices, as seen in the following equations, are represented in Voigt notation, which translates symmetric tensors to six-dimensional vectors.

In order to map the stiffness matrix from the natural coordinate system to the physical coordinate system in Equation 1.6, the $\det(J)$ factor is used (Liu, 2014). This is done by taking the location values from the physical coordinate system and multiplying them with the change of the shape functions in each location of natural coordinate system, represented by Equation 1.9. With all variables in Equation 1.6 defined, the stiffness matrix for the element is formulated. With this value, we can then calculate the displacements of all the nodes in each element through Equation 1.5. These displacements will then be used to determine the mean compliance, which will be used to inform the TO material removal process. This process will be described in the following section.

$$J = \begin{bmatrix} \frac{\partial N_1}{\partial \alpha} & \frac{\partial N_2}{\partial \alpha} & \frac{\partial N_3}{\partial \alpha} & \frac{\partial N_4}{\partial \alpha} & \frac{\partial N_5}{\partial \alpha} & \frac{\partial N_6}{\partial \alpha} & \frac{\partial N_7}{\partial \alpha} & \frac{\partial N_8}{\partial \alpha} \\ \frac{\partial N_1}{\partial \beta} & \frac{\partial N_2}{\partial \beta} & \frac{\partial N_3}{\partial \beta} & \frac{\partial N_4}{\partial \beta} & \frac{\partial N_5}{\partial \beta} & \frac{\partial N_6}{\partial \beta} & \frac{\partial N_7}{\partial \beta} & \frac{\partial N_8}{\partial \beta} \\ \frac{\partial N_1}{\partial \gamma} & \frac{\partial N_2}{\partial \gamma} & \frac{\partial N_3}{\partial \gamma} & \frac{\partial N_4}{\partial \gamma} & \frac{\partial N_5}{\partial \gamma} & \frac{\partial N_6}{\partial \gamma} & \frac{\partial N_7}{\partial \gamma} & \frac{\partial N_8}{\partial \gamma} \end{bmatrix} \begin{bmatrix} x_1 & y_1 & z_1 \\ x_2 & y_2 & z_2 \\ x_3 & y_3 & z_3 \\ x_4 & y_4 & z_4 \\ x_5 & y_5 & z_5 \\ x_6 & y_6 & z_6 \\ x_7 & y_7 & z_7 \\ x_8 & y_8 & z_8 \end{bmatrix} \tag{1.9}$$

2

Topology Optimization

2.1 Overview of Topology Optimization

This section shall give an overview of the SIMP and BESO TO methods to give a better understanding of how each method redistributes material based on FEA results. All TO methods have two goals in mind when solving structural optimization problems: find the minimum mean compliance and fit within a given target volume.

$$C = \sum_{i}^{N} \frac{1}{2} u_i K_i u_i^T \tag{2.1}$$

The mean compliance of the entire structure can be represented by equation 2.1, where u_i represents the elemental displacement matrix, K_i is the stiffness matrix of the element, u_i^T is the transpose of the elemental displacement matrix, and N is the number of elements in the structure Huang (2008). As we minimize this value — there are fewer deformations in the structure, resulting in a stronger structure [1].

$$V^* - \sum_{i}^{N} V_i x_i = 0 \tag{2.2}$$

Alongside this, TO methods also try to fit within a given target volume. This value is specified at the beginning of the optimization process. Each TO methods redistributes material in order to try to satisfy Equation 2.2, where V^* represents the target volume, V_i represents the elemental volume, x_i represents the design variable that determines whether that element exists or not in the current design, and N is the number of elements in the structure. TO Methods iterate until the volume

[1] Compliance essentially represents the strain energy density as described by Equation 1.4. This tells us how much strain energy there is in the system.

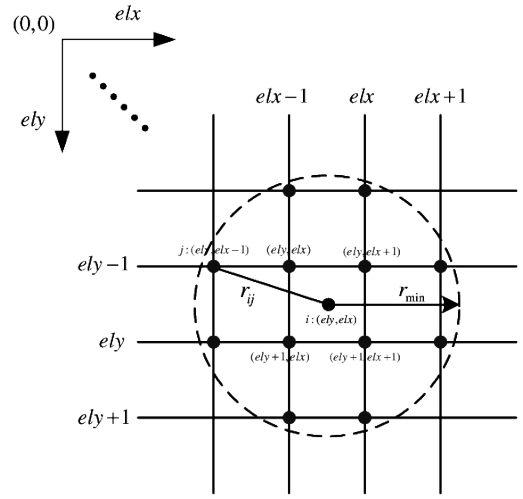

Figure 2.1: **Two dimensional slice of filter radius** (Wang et al., 2011). A filter radius, commonly known as r_{min} encapsulates a certain amount of area or volume within a structure. From the center of each element, TO methods look r_{min} distance out. Within this circle or sphere, certain nodes with sensitivity values are encapsulated. Based on the average of these values we can determine how stiff the system is in this region is.

condition is met and then continues to redistribute material in order to minimize the compliance of the entire structure. TO methods typically determine how to redistribute based on the principle of neighboring elements. At the beginning of the optimization process, the user specifies what is known as the filter radius. This value determines how far the optimization methods should look in terms of number of elements out. This helps determine whether certain regions in the structure need more support or could potentially be cut. Figure 2.1 shows a two-dimensional slice of what a filter radius looks like. During the removal or addition process in topology optimization, each element looks a certain filter radius outward. In the two-dimensional case we see through Figure 2.1 that certain nodes are encapsulated in this region. We average each of these nodal sensitivity values to determine how stressed this area is and use this information in the decision making process. However, each topology optimization method redistributes material in its own way.

2.2 Solid Isotropic with Material Penalization (SIMP)

The SIMP method views the design variable, x_i, as a continuous value, that allows for what I call *partial elements*. The design variable is allowed to have a continuous density value that follows the inequality expressed by Equation 2.3, where x_{min} is

the minimum element density allowed and x_i is the element density.

$$0 < x_{min} \leq x_i \leq 1 \tag{2.3}$$

Any design variable that falls below the x_{min} value is removed from the design and becomes known as a *void* element. Any design variable that converges to the value 1 becomes known as a *solid* element. Anything else in between is a partial element. In order to determine these design variables at every iteration, the SIMP method calculates sensitivity values. This is done by taking the derivative of the mean compliance, such that

$$\frac{\partial c}{\partial x_i} - p x_i^{p-1} u_i^T K_i^0 u_i \tag{2.4}$$

where p represents a penalty factor (typically 2 or 3)[2], x_i represents the design variable of the element, u_i^T represents the transposed displacement matrix of the element, K_i represents the stiffness matrix of the element, and u_i represents the displacement matrix. Using this value, we can calculate the amount of volumetric change in dimensions of the element by calculating the strain through Equation 2.5, where λ^{-1} is a Lagrangian multiplier determined through a bisection method (M. P. Bendsøe, 1999).

$$B_i = \lambda^{-1} \frac{\partial c}{\partial x_i} \tag{2.5}$$

Using this change in mean compliance, we can then update the elements through Equation 2.6, which represents the Optimality Criteria described by M. P. Bendsøe (1999).

$$x_i^{N+1} = \begin{cases} max(x_{min}, x_i^N - m) & \text{if } x_i^N B_i^\eta \leq \ max(x_{min}, x_i^N - m) \\ min(1, x_i^N + m) & \text{if } min(1, x_i^N + m) \leq x_i^N B_i^\eta \\ x_i^N B_i^\eta & \text{otherwise} \end{cases} \tag{2.6}$$

where x_i^N represents the design variable at iteration N, m is the positive move limit — the most the value can change per iteration, η represents a numerical damping coefficient (typically equal to 0.5), and B_i is elemental strain. With the sensitivity values being based upon the change of compliance with respect to the design variable, it has been noted by Huang (2008) to sometimes converge to local minimums — which may cause for less than optimal designs.

[2]This intrinsically helps the design to a fully solid design.

2.3 Bi-directional Evolutionary Structure Optimization (BESO)

The bi-directional evolutionary structure optimization (BESO) is a bit different in nature than the SIMP method. The BESO method was an adaptation from the evolutionary structure optimization (ESO) method, which was first developed by X. Y. Yang and Querin. (1999). The term *"bi-directional"* implies that material can be both added and subtracted at the same time, meaning inefficient material is removed from the design and material is added in places needed of more support. This allows the method to redistribute material in the design where it may have previously pre-maturely subtracted it. The BESO method also works on the premise of sensitivity values. Each sensitivity value is the mean compliance divided by the elemental volume, as seen in Equation 2.7

$$\alpha_i = \frac{1}{2}\frac{u_i^T K_i u_i x_i^p}{V_i} \tag{2.7}$$

u_i is the displacement matrix of the element, u_i^T is the transposed displacement matrix of the element, and K_i is the stiffness matrix for that given element, x_i is the design variable, and p is the penalty factor (typically 2 or 3) used for helping the design converge. These sensitivity values are compared to a threshold value, a_{th}, the mean value of sensitivity values across the nodes within the given filter radius of the element. If the design variable is 1, then the element exists in the design, if the element is 0.001 it has the potential to to be added back into the design, if the design variable is less than 0.001 it is completely removed from the design — continuously becoming smaller and smaller each iteration.

$$x_i = \begin{cases} 1 & \text{if } a_i > a_{th} \\ 0.001 & \text{if } a_i \leq a_{th} \end{cases} \tag{2.8}$$

This method continuously subtracts material from the structure at an evolutionary rate, the rate at which elements are removed from the structure. Once the structure is at its target volume, V^*, it still can continue to redistribute material without changing the overall volume of the structure, adding and subtracting material for optimum results. However, it has been noted in literature that by adding a penalization factor to the design variable causes for more convergent solutions (Huang, 2008).

3

Computational & Analytic Results

3.1 Validation of Finite Element Analysis

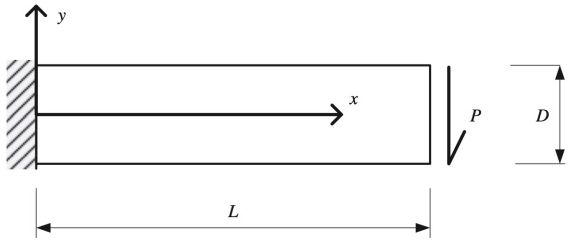

Figure 3.1: **Cantilever beam validation test setup.** (Augarde, 2007) This represents a two-dimensional model of the Timoshenko cantilever beam described by Auguarde. The beam consists of length, L, a height, D, and shear force, P, in the downwards direction.

For the structures generated by the BESO method, FEA software was written in order to define the displacements, stress, and strain in the system. The FEA software works on the premise of Lagrange shape functions, as described in Section 1.3. In order to validate this approximation, we will compare the displacement results with an analytic solution of the cantilever beam as described by Augarde (2007). The cantilever described by Augarde represents a two-dimensional cantilever beam of depth, D, length, L, and unit thickness as seen in Figure 3.1. A load, P, is set upon the end of the beam in order to deform the structure. To quantify the deformation in the y-direction, we look at u_y, as described in Equation 3.1, where ν is Poisson's ratio and I is the moment of area. This beam theory is derived from the Euler-Bernoulli Beam Theorem.

$$u_y = -\frac{P}{6EI}\left[3\nu y^2(L-x) + (4+5\nu)\frac{D^2 x}{4} + (3L-x)x^2\right] \tag{3.1}$$

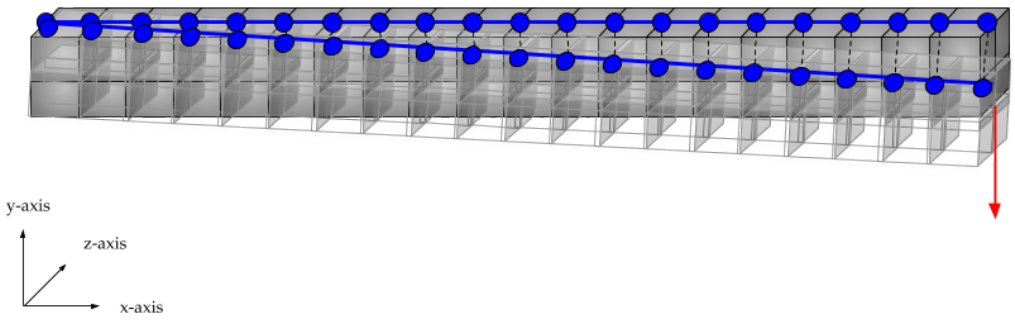

Figure 3.2: **Validation test scenario: FEA Setup.** The y-displacement from the top row of nodes that are centered with the load will be used to compare with the y-displacement of the Timoshenko beam model.

The FEA software written for the BESO method solves only three-dimensional systems. In order to compare this to the Timoshenko model, we shall use a simple test scenario as shown in Figure 3.2. This Figure shows a cantilever beam under a given load composed of 80 elements (20 x 2 x 2). Using this model, we can compare the y-displacements to the Timoshenko beam model to see how accurate the FEA solution is. To give some physical context, the defined parameters that were used in this validation test is given below in Table 3.1, which describes a steel cantilever beam with a given load of 1000 N set up on it.

Length (mm)	20
Depth (mm)	2
Load (N)	1000
Elastic Modulus $(\frac{N}{m^2})$	200e9
Poisson's Ratio (ν)	0.4

Table 3.1: Validation test parameters: FEA vs. Analytic Solution

Under this scenario, it was seen in Figure 3.2 that the displacements predicted by the FEA software had deflected further in the y-direction in comparison to the Timoshenko analytic solution. This tells us that although the FEA predicted the correct sort of shape of the displacement and direction in which the beam shall be displaced, it over approximated the amount of displacement in the system. As you get further towards the end of the beam, the error margin of this approximation continues to increase.[1]

[1] Although the FEA software has a significant error margin in comparison to the analytic solution, it should suffice for the optimization methods.

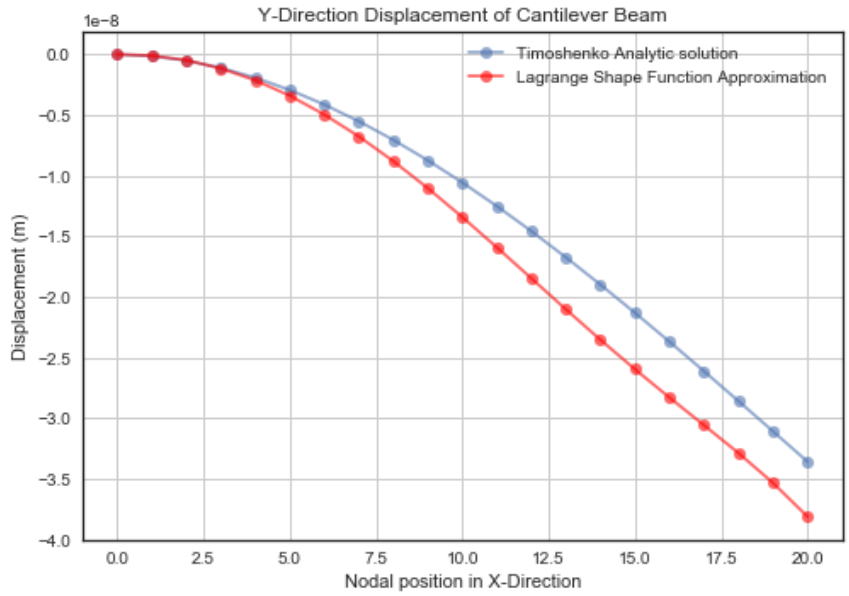

Figure 3.3: **Y-displacement comparison of analytic solution and FEA solution.** This shows the displacement of a cantilever beam from both the Auguarde analytic solution compared to the FEA solution as it bends in the y-direction. From the comparison, we see that the minimum error in the FEA approximation is 4.28×10^{-11} m and the maximum error is 4.65×10^{-9} m. Relative to the solution this error in displacement ranges from 3.93% to 27.18%, with the average relative error being 16.50%.

3.2 Topology Optimization Results

To compare the SIMP and BESO method fairly, a common scenario shall be used to design a cantilever beam. The common parameters for this validation scenario can be seen in Table 3.2. We will compare several different structures at various volume fractions in Section 3.3, but for the sake of brevity this paper shall only discuss the optimization process of structures generated with a target volume of 15%. For each TO method, mean compliance over time shall be analyzed to how effective each method is during its optimization period. This analysis shall show pivotal changes in design at particular iterations to compare each method during its optimization process.

Length	40
Width	12
Height	20
Target Volume	15%
Elastic Modulus	200e9
Filter radius	1.5

Table 3.2: Design scenario: Common initial parameters

3.2.1 SIMP Method Optimization Results

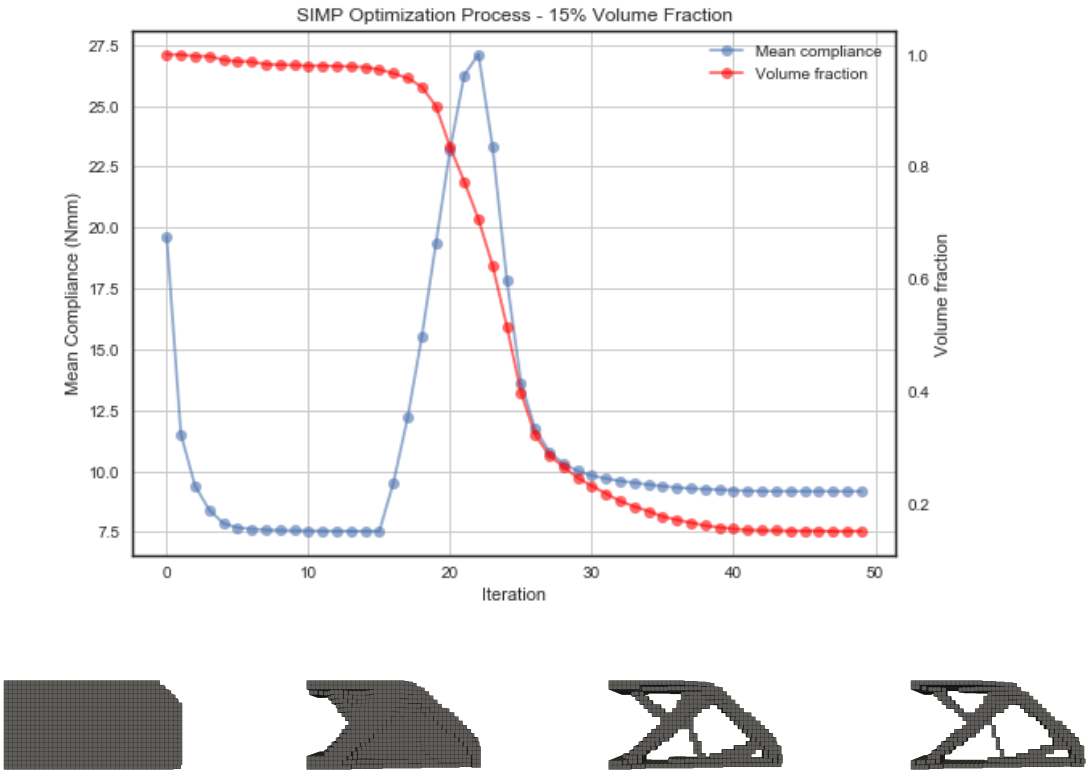

(a) Iteration 15 (b) Iteration 25 (c) Iteration 35 (d) Iteration 50

Figure 3.4: **SIMP Method Optimization Process.** The optimization process was completed relatively quickly — converging to a solution in less than fifty iterations. From the graph, it shows the method was relatively conservative when subtracting material in the first half of the optimization process, until it quickly subtracts a lot of material. This is due to the move limit being fixed for the first fifteen iterations of the optimization process — preset by the ToPy (Hunter, 2009). The final structure had a mean compliance of 9.16 Nmm, resulting in a structure as seen in Figure d.

Figure 3.4 shows the optimization process results for the SIMP method that was generated using the ToPy Python library (Hunter, 2009). For each iteration, a small percentage of material is subtracted from the overall design based upon the change in mean compliance, as described in Section 2.3. In the beginning of the optimization process, one notices that the overall change in volume fraction is relatively small. However, as we see from point b to point c in Figure 3.4 there is a rapid change in the volume fraction, where the overall change in volume is quite high — this corresponded to a rise in compliance. As the process converged to the target volume we see the mean compliance becomes minimized. Higher resolution multi-dimensional images of this structure can be seen in Section 3.2.3.

3.2.2 BESO Method Optimization Results

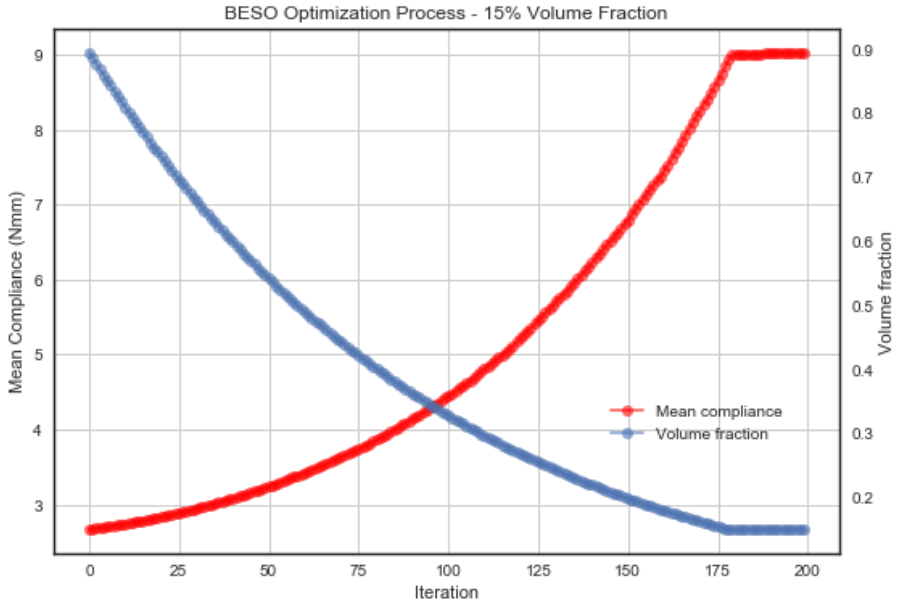

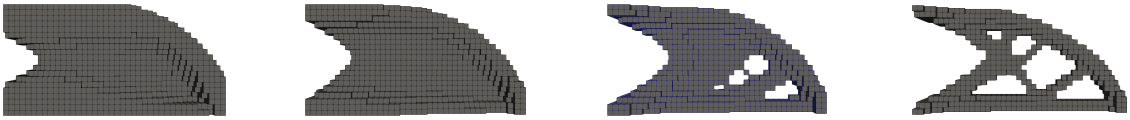

(a) Iteration 30 (b) Iteration 81 (c) Iteration 137 (d) Iteration 188

Figure 3.5: **BESO Method Optimization Process.** The BESO method took longer to come to an optimal solution — 188 iterations based off an evolutionary rate of 1% volume fraction per iteration. The resulting mean compliance was 9.03 Nmm, resulting in a structure that looks similar to Figure d. This behavior in the BESO method is consistent with literature described by *Evolutionary Topology Optimization of Continuum Structures* (Huang, 2008), such that as volume fraction decreases, mean compliance increases.

Figure 3.5 shows the optimization process for the BESO method that was generated by software, which can be found at this link. This process is a little more straightforward in comparison to the SIMP method, as the volume fraction is determined by a fixed evolutionary rate. This means instead of determining how much material to subtract from the structure based on the change in mean compliance of the structure, it subtracts material at fixed rate. However, instead of just subtracting material like the SIMP method, the BESO method redistributes or *"adds"* material to support weaker areas, so long as the total volume fraction is reduced by the evolutionary rate. This feature is not inherent to the SIMP method, which might prematurely subtract material in areas that might prove to be weak in future iterations.

3.2.3 3D Voxel Renderings of SIMP vs. BESO

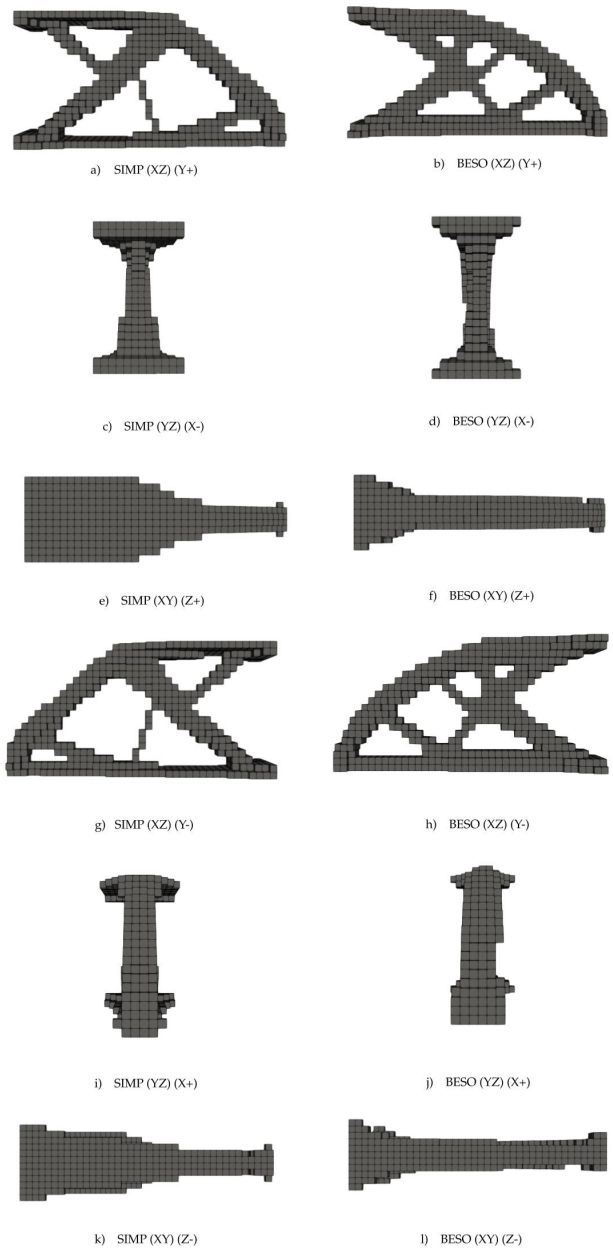

Figure 3.6: **Comparison of SIMP and BESO 3D Voxel Renderings** The resulting structures have relatively similar features, including an overarching structure as seen in Figure a, b, g, and h. However, we see that the SIMP method more aggressively subtracted material from the interior portions of it's design, leaving more material on the top and bottom of the design as seen in Figures e , f, k, and l . Both structures had I-beam shaped back features — as seen in Figures c and d — this is reassuring that human design isn't *that bad*. It is also noted that the BESO method produced slightly asymmetrical designs most notably in front and back views.

3.2.4 Qualitative Discussion of BESO vs. SIMP Results

From the TO results highlighted in Sections 3.2.1 and 3.2.2, we see that the TO methods converged to relatively similar structures. Both structures had the same overarching shape with material removed near the fixed portion of design as seen in Figure 3.6a, 3.6b, 3.6g, and 3.6h. Both structures reduced to a I-beam shaped structure near the back of the design as seen in Figure 3.6c and 3.6d. This is quite relieving to see that human design matches what these methods generate. Each structure has interior cuts in order to reduce volume, however each method did it in its own way. The BESO method seems to make smaller cuts and remove more material from the top of the structure, whereas the SIMP method subtracted a lot more interior material in the interior portions of structure causing a bigger gap. The BESO method had small asymmetries as seen in Figure 3.6j and 3.6d. Each facet of these designs will be analyzed in further sections to determine whether each method made the correct decision in redistributing material in specific areas.

3.3 Static Load Analysis of SIMP vs. BESO

In order to fairly compare each structure generated by the SIMP and BESO methodologies, a known finite element analysis suite, AutoDesk, was used to simulate static load scenarios. In order to create a valid mesh in AutoDesk, each structure had to be modified to be a smoothed surface. This was done by applying a Poisson Surface Reconstruction (PSR) filter. The modified structures can be seen Appendix B and can be compared with the voxel renderings as seen in Figure 3.5. Although it's not ideal to compare modified structures, a large effort was put into ensuring the structure's design was preserved. Each structure underwent a static load for the scenario that it was designed for, as described in 3.2. From this analysis, a comparison of the set of criterion below in the list will be utilized to determine which TO methodology produced a better structure.

1. Von Mises Stress
2. Strain
3. Displacement
4. Euler Critical Load

TO Method Vol. Frac.	Max Strain	Avg. Strain	Max Stress (MPa)	Avg. Stress (MPa)	Max Displacement (mm)	Avg. Displacement (mm)
BESO - 15%	3.28E-5	3.08E-6	4.392	0.561	4.89E-3	1.39E-3
SIMP - 15%	2.23E-5	5.30E-6	3.988	0.764	5.65E-3	2.35E-3
BESO - 25%	2.80E-5	2.91E-6	3.687	0.476	3.16E-3	9.21E-4
SIMP - 25%	1.85E-5	3.6E-6	2.526	0.612	4.60E-3	2.24E-3
BESO - 35%	1.19E-5	3.41E-6	1.735	0.477	3.47E-3	1.26E-3
SIMP - 35%	3.09E-5	3.49E-6	4.246	0.548	3.78E-3	1.70E-3
BESO - 45%	8.10E-6	2.52E-6	1.269	0.362	2.71E-3	9.24E-4
SIMP - 45%	1.35E-5	2.07E-6	1.803	0.308	2.20E-3	8.81E-4
BESO - 55%	1.18E-5	1.93E-6	1.641	0.273	2.23E-3	7.63E-4
SIMP - 55%	1.17E-5	1.19E-6	1.532	0.273	1.83E-3	7.2E-4

Table 3.3: **Quantitative Results from Static Load Analysis** This table represents the results from the AutoDesk static load test for each method and volume fraction. From initial glance it is evident that the BESO method outperforms the SIMP method in terms of average stress, strain, and displacements for volume fractions below 35%, whereas the SIMP outperforms the BESO method for volume fractions 45% and above.

The results from the static load scenarios are shown in Table 3.3. Each structure generated by both the BESO and SIMP method were put under a 1000 N load, in a similar fashion to the FEA validation scenario in Figure 3.2. Then each structure was tested to its limits, until the structure buckled — giving us the Euler Critical load. To conduct the simulation, each structure was converted to a mesh consisting of 2,000 uniform faces for consistency. From initial glance, it seems as though each structure for the most part linearly continues to improve in terms of stress, strain, displacement — as we see these number effectively decrease as more material is added to the structure. However, it must be noted that with the mesh conversion, there may be some slight effects in the performance of the structure. We may notice that specifically thin connections in the the lower volume fraction designs may encounter higher areas of stress than they were in their voxel form. To further investigate and understand the results listed in Table 3.3, color maps of stress, strain, and displacement for each structure will be shown in the following sections. This ultimately will help us understand where each structure is weakened and help us determine if structural flaws could have influenced some of the quantitative results as seen in Table 3.3.

3.3.1 Von Mises Stress and Strain Analysis

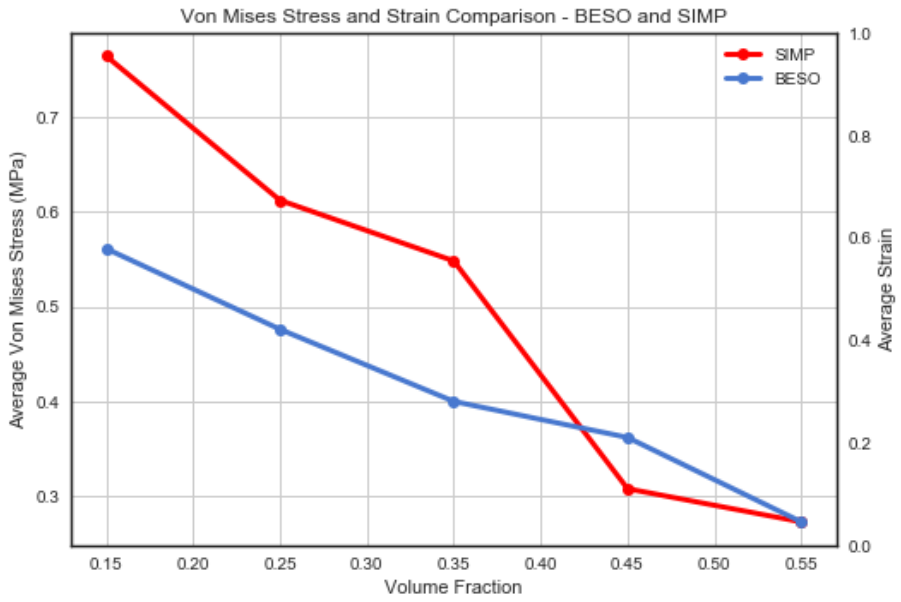

Figure 3.7: **Average Stress and Strain vs. Volume Fraction.** The BESO method showed high areas of stress in low volume fractions — particular in the thin connections. However, on average it outperformed the SIMP method slightly for lower volume fractions. We see the SIMP method do slightly better in higher volume fractions — both methods have similar average stress for the 55% volume fraction optimization.

Table 3.4 shows the Von Mises stress map for each structure generated by the BESO and SIMP methods at different target volumes. With these stress maps, we can view where the structure is weakest. One may notice that the greatest amount of stress across the structures are the thin connections, most notable in the smaller volume fractions of the SIMP and BESO design structures. It shall be noted that when these structures are converted to a mesh from the PSR structures, they often are reduced by small volume. This may lead to connections to become thinner than they were in the original design. This causes the structure in these areas to feel higher amounts of stress than they normally would.

We can also look at the average amount of stress across each structure. If we plot the average Von Mises stress values for each structure at each volume fraction, as seen in Figure 3.7, we can see that the BESO on average has a lower stress and strain profile in comparison than the SIMP method for value fractions below the 45% volume fraction mark. At this point, the SIMP on average performs better. This potentially could tell us that the SIMP method works for higher volume fraction, whereas the BESO works better for lower volume fractions.

Volume Fraction	SIMP	BESO
15%	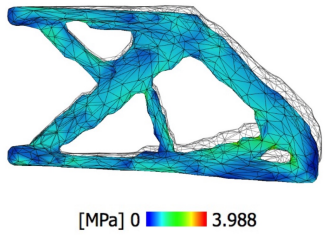	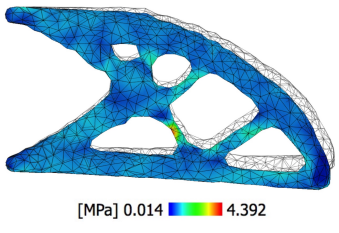
25%	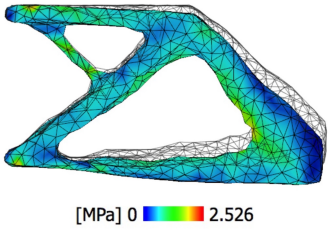	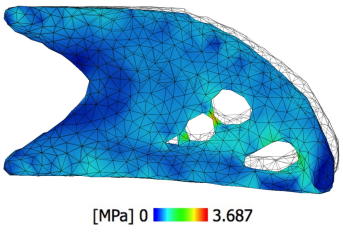
35%	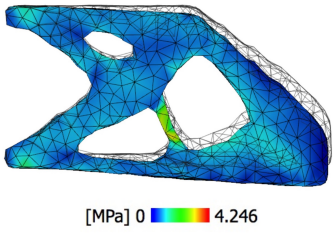	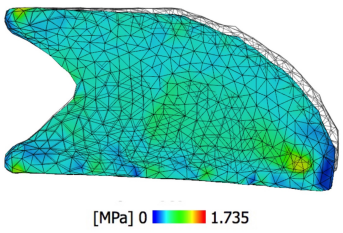
45%	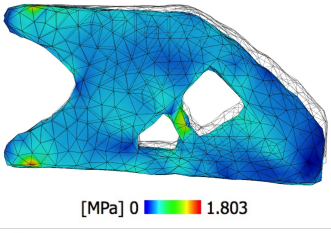	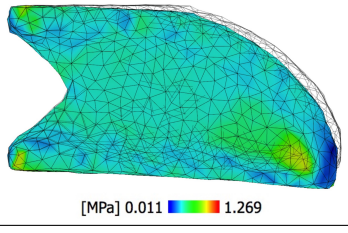
55%	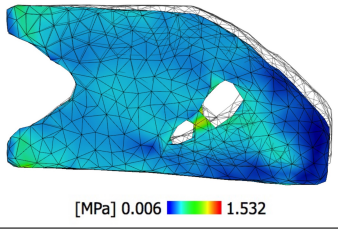	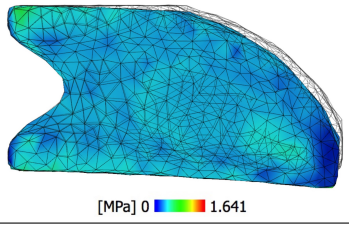

Table 3.4: **BESO vs. SIMP Von Mises Stress Comparison.** This table highlights the stress simulation results from AutoDesk for each method and target volume done. We see that there are notable areas within the structure that suffer higher amounts of stress, namely in areas where connections are thin as seen in lower volume fractions.

3.3.2 Displacement Analysis

Volume Fraction	SIMP	BESO
15%	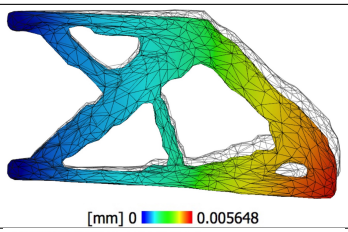	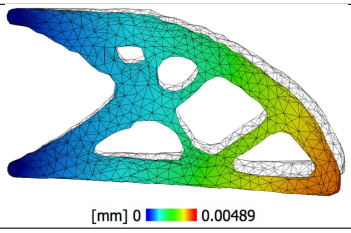
25%	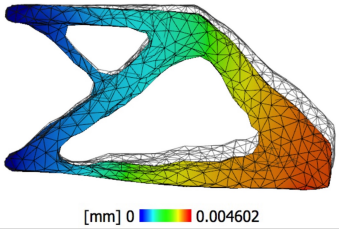	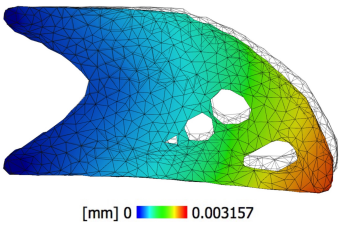
35%	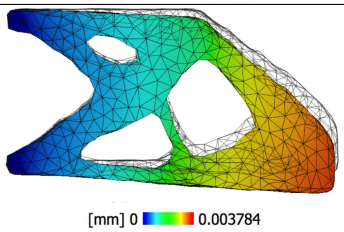	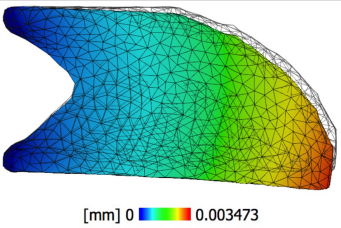
45%	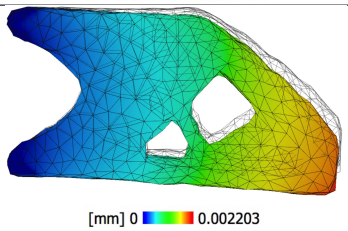	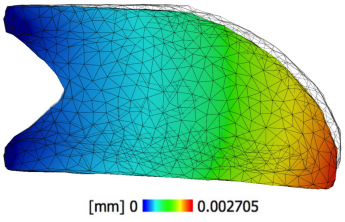
55%	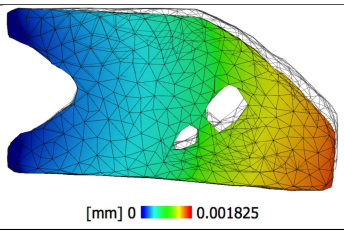	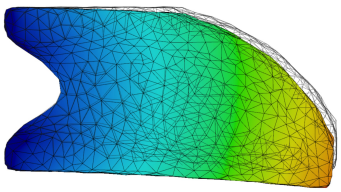

Table 3.5: **BESO vs. SIMP Average Displacement Comparison.** This table shows the results from the average displacement analysis results from AutoDesk. The SIMP at lower volume fractions seemed to encounter higher values of displacement in comparison to the BESO method. The SIMP however, seems to feel less displacement at higher volume fractions.

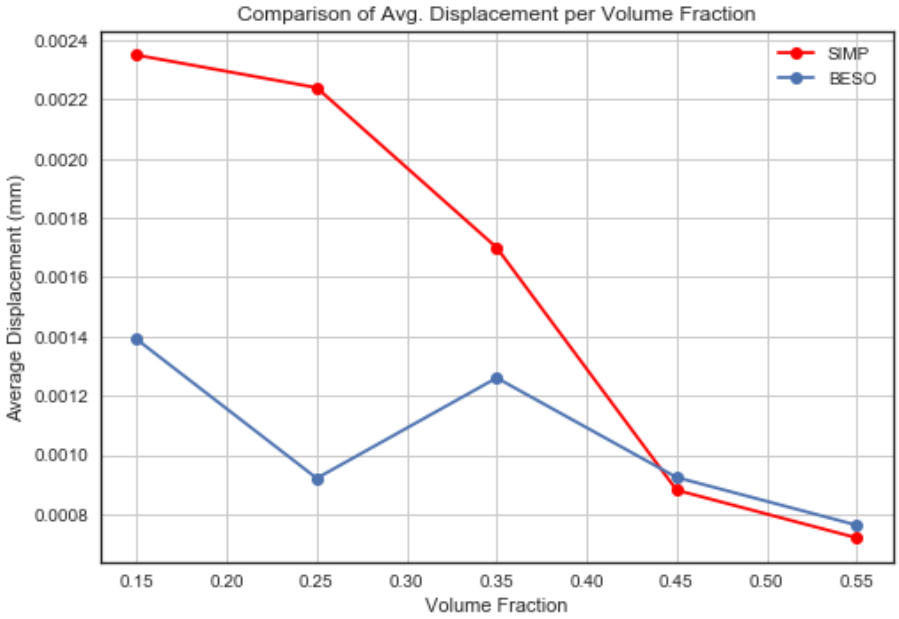

Figure 3.8: **Average Displacement for each TO method and volume fraction.** The SIMP on average had much higher displacements for low volume fractions. However, we start to see the SIMP perform very similar higher volume fractions.

Comparing the average displacements of the structures in Figure 3.8a we also notice that the trend from the stress and strain graphs are consistent. However, the shape of this graph is slightly different, which may suggest some sort of weighted average was used in the calculations calculated by AutoDesk. The average displacements are much larger for the SIMP method in comparison to the BESO method for volume fraction of 15-35%. It is only until 45-55% where the SIMP barely performs better than the BESO method. The displacements can be viewed in Table 3.5, which shows adjusted views of the displacements for each structure generated by the SIMP and BESO methods.

3.3.3 Euler Critical Load Analysis

From first glances in Figure 3.9, it seems as though that the SIMP vastly outperformed the BESO method in terms of Euler critical load in volume fractions between 45-55% as seen in Figure 3.8b. In contrast, the BESO slightly outperforms the SIMP method from 15-35% for Euler critical loads. This helps support the idea that the BESO method is better at lower volume fractions for the cantilever beam design in comparison to the SIMP method. However from Figure 3.9, we see that the BESO method is very close in performance to the SIMP at the 15% volume fraction. This may be explained by the thin connection as seen in the 15% volume fraction BESO

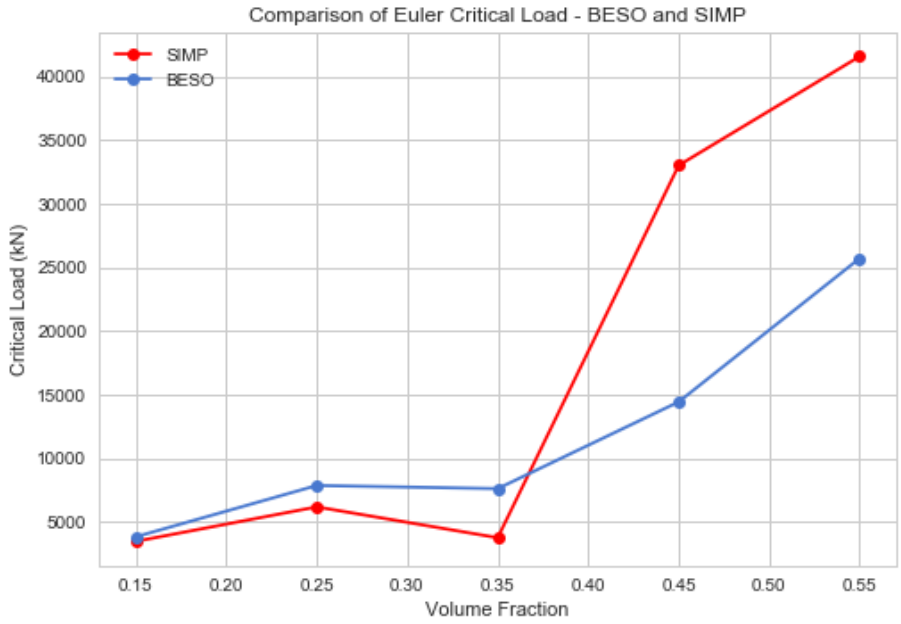

Figure 3.9: **Euler Critical Load for each TO method and volume fraction.** It is observed that the SIMP method vastly outperformed the BESO methods in terms of Euler critical load at higher volume fractions of 45-55%.

TO Method Vol. Frac.	Euler Critical Load (kN)
BESO - 15%	3811
SIMP - 15%	3453
BESO - 25%	7844
SIMP - 25%	6162
BESO - 35%	7596
SIMP - 35%	3739
BESO - 45%	14416
SIMP - 45%	33000
BESO - 55%	25698
SIMP - 55%	41563

Table 3.6: **Euler Critical Load.** The volume BESO barely held more weight than the SIMP method at lower volume fraction, however the SIMP method vastly outperformed the BESO method at higher volume fractions.

design, where the maximum stress is higher than that of the SIMP method, which may have caused it to prematurely break. This thin connection could be a result of voxel to mesh conversion, however there is still room for speculation in which will be discussed in the next section.

4

Conclusion

4.1 Discussion

4.1.1 Finite Element Analysis

From the results listed in Section 3.1 we saw that the FEA software used by the BESO method to calculate the displacements in the cantilever beam had performed similarly to the Timoshenko analytic solution derived from Euler beam theory. The error in the FEA solution ranged from 4.28×10^{-11} -4.65×10^{-9} m. This translated to an average of 16.50% relative error between the analytic solution and the FEA Lagrange shape function solution. Although this is not ideal, it served its purpose for the computational experiment. In speculation, this comparison is in itself an approximation through comparison of a 2D and 3D model. Therefore, we might have seen the solution align more closely if we compared this software with a 3D analytic solution.

4.1.2 Optimization Processes

From the optimization processes, we ultimately saw that the SIMP converged much faster than the BESO method. This was ultimately due to the evolutionary rate that was chosen for the BESO method in which caused it to subtract material off at a slower rate, whereas the SIMP method subtracted material at a variable rate based upon the relationship described in Equation 2.8. We saw that overall the optimized structures converged to relatively similar structures, with overarching FEATURES and an I-beam shaped back. From this we qualitatively viewed how each method chose to subtract material. The BESO decided to take smaller cuts

from the interior material and subtract material from the top, whereas the SIMP method subtracted much of the material from the interior and left one big gap. This resulted in more material on top of the structure. This suggests that the SIMP may have prematurely subtracted material. We also noticed that the BESO suffered from some minor asymmetries in the final structure.

4.1.3 Static Load Analysis

From what we saw in the static load analysis was that the BESO outperformed the SIMP method in terms of stress, strain, displacement, and Euler critical load at target volumes from 15-35% volume fraction — claiming itself the more *"effective"* structure for low volume fractions. Alongside the BESO method, the SIMP method outperformed the BESO method for volume fractions between 45-55% target volumes — marking itself the more *"effective"* structure for higher volume fractions.

However, these results are open to speculation. There is a certain amount of uncertainty of how much effect the conversion between voxel and smoothed mesh played a role into the performance of each structure. When each structure was converted to a smoothed mesh, each structure may have been reduced by a small volume. This was especially most notable in designs that had thinner connections as seen in the lower volume fraction structures. This made certain aspects of the design to encounter higher amounts of stress, which potentially could lead to the structure to support less load.

4.2 Future Research

This was just a small fraction of many of the different tests we could have run in order to compare the two TO methods. To get a better understanding between how these two methods compare, a larger data set of many different types of structures such as the bridge and the truss would have to be compared. This would help us see if the observations we saw in the cantilever beam would hold true for other structures or perhaps give us insight to whether or not a particular method is better for a particular structure.

Improvements to the BESO software could be made to make it more memory efficient. As of now it takes up so much of memory that it requires swap space to be used — causing the software to take a very long time as well. An effort to convert the software to use sparse matrices was undertaken, but the results did not come out

quite as expected. Further investigation in finding a solution that supports sparse matrices would make the software both more memory efficient and computationally efficient.

4.3 Ending Notes

This thesis paper has shown that TO methods can provide unique geometries that ultimately lead to highly optimized designs. Using computers and TO methods to create designs will become more common as our manufacturing techniques become cheaper in the future. There is a lot of work to be done before these methods are more fully understood, but as we continue to study these methodologies a new era of design will emerge — and perhaps we will find more things that we could have never possibly imagined.

Bibliography

Augarde, Charles E., D. A. J. (2007). The use of timoshenko's exact solution for a cantilever beam in adaptive analysis. . Accessed 2019/04/11.

Huang, X., . X. Y. M. (2007). Convergent and mesh-independent solutions for the bi-directional evolutionary structural optimization method. finite elements in analysis and design. . Accessed 2018/03/25.

Huang, X., . X. Y. M. (2009). Bi-directional evolutionary topology optimization of continuum structures with one or multiple materials. computational mechanics. . Accessed 2018/03/25.

Huang, X., X. Y. M. (2008). *Evolutionary Topology Optimization of Continuum Structures: Methods and Applications*. Accessed 2019/04/17.

Hunter, W., . G. A. A. (2009). Predominantly solid-void three-dimensional topology optimisation using open source software. . Accessed 2018/03/25.

Kai Liu, A. T. (2013). An efficient 3d topology optimization code written in matlab. . Access 2018/03/30.

Leonard, D. (2018). New design approach: Interplanetary landers. Accessed 2019/05/10.

Liu, G. R. (2014). *The Finite Element Method: A Praticle Course*. Accessed 2019/04/16.

M. P. Bendsøe, O. S. (1999). Material interpolation schemes in topology optimization. . Access 2018/03/30.

Taylor, J. R. (2005). *Classical Mechanics*. University Science Books. Accessed 2019/01/28.

Wang, Q., Zhenzhou, L., and Zhou, C. (2011). New topology optimization method for wing leading-edge ribs. *Journal of Aircraft*, 48:1741–1748.

X. Y. Yang, Y. M. Xei, G. P. S. and Querin., O. M. (1999). Bidirectional evolutionary method for stiffness optimization. . Accessed 2019/03/31.

Xia, L., X. Q. H. X. . X. Y. M. (2018a). Bi-directional evolutionary structural optimization on advanced structures and materials: A comprehensive review. archives of computational methods in engineering. . Accessed 2018/03/25.

Xia, L., Z. L. X. Q. . S. T. (2018b). Stress-based topology optimization using bi-directional evolutionary structural optimization method. computer methods in applied mechanics and engineering. . Accessed 2018/03/25.

Xie, Y. M., . H. X. (2014). Recent developments in evolutionary structural optimization (eso) for continuum structures. in iop conference series: Materials science and engineering. . Accessed 2018/03/25.

Young, V., Q. O. M. S. G. P. . X. Y. M. (1999). 3d and multiple load case bi-directional evolutionary structural optimization (beso). structural optimization. . Accessed 2018/03/25.

Appendix A

Finite Element Analysis Lagrange Interpolation

A.1 Shape Functions

$$N_1 = \frac{1}{8}(1-\alpha)(1-\beta)(1-\gamma) \tag{A.1}$$

$$N_2 = \frac{1}{8}(1+\alpha)(1-\beta)(1-\gamma) \tag{A.2}$$

$$N_3 = \frac{1}{8}(1+\alpha)(1+\beta)(1-\gamma) \tag{A.3}$$

$$N_4 = \frac{1}{8}(1-\alpha)(1+\beta)(1-\gamma) \tag{A.4}$$

$$N_5 = \frac{1}{8}(1-\alpha)(1-\beta)(1+\gamma) \tag{A.5}$$

$$N_6 = \frac{1}{8}(1+\alpha)(1-\beta)(1+\gamma) \tag{A.6}$$

$$N_7 = \frac{1}{8}(1+\alpha)(1+\beta)(1+\gamma) \tag{A.7}$$

$$N_7 = \frac{1}{8}(1+\alpha)(1+\beta)(1+\gamma) \tag{A.8}$$

$$N_8 = \frac{1}{8}(1-\alpha)(1+\beta)(1+\gamma) \tag{A.9}$$

Appendix B

Poisson Surface Reconstructed Structures

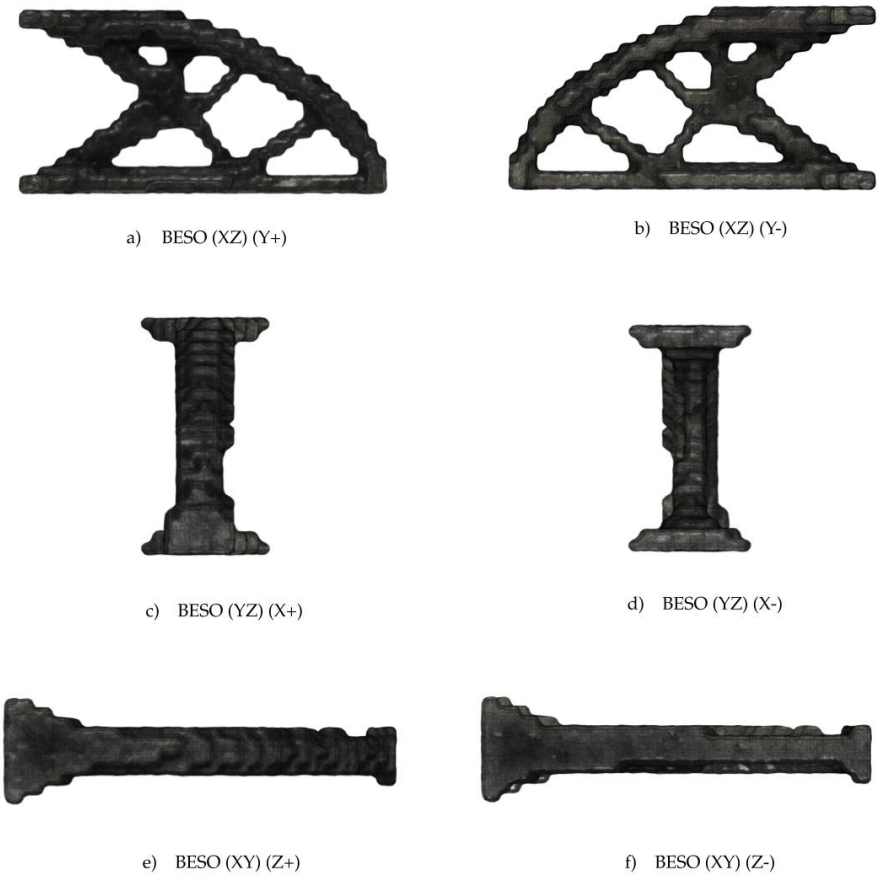

Figure B.1: 15% VF BESO Cantilever with PSR Filter

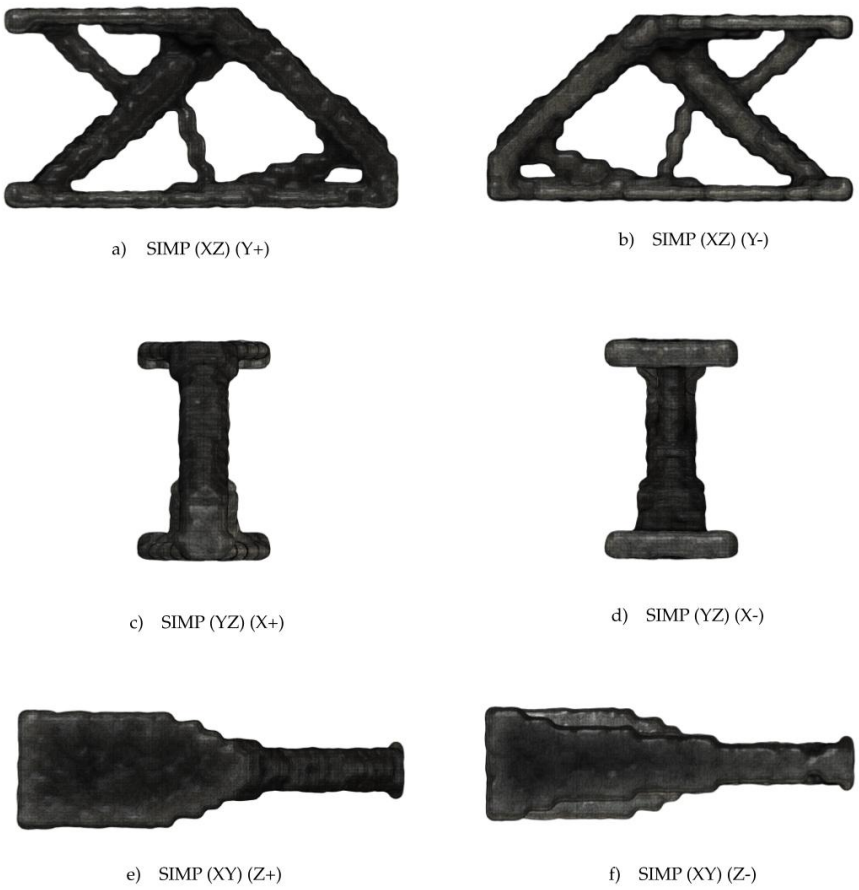

Figure B.2: 15% VF SIMP Cantilever with PSR Filter

Figure B.3: 25% VF BESO Cantilever with PSR Filter

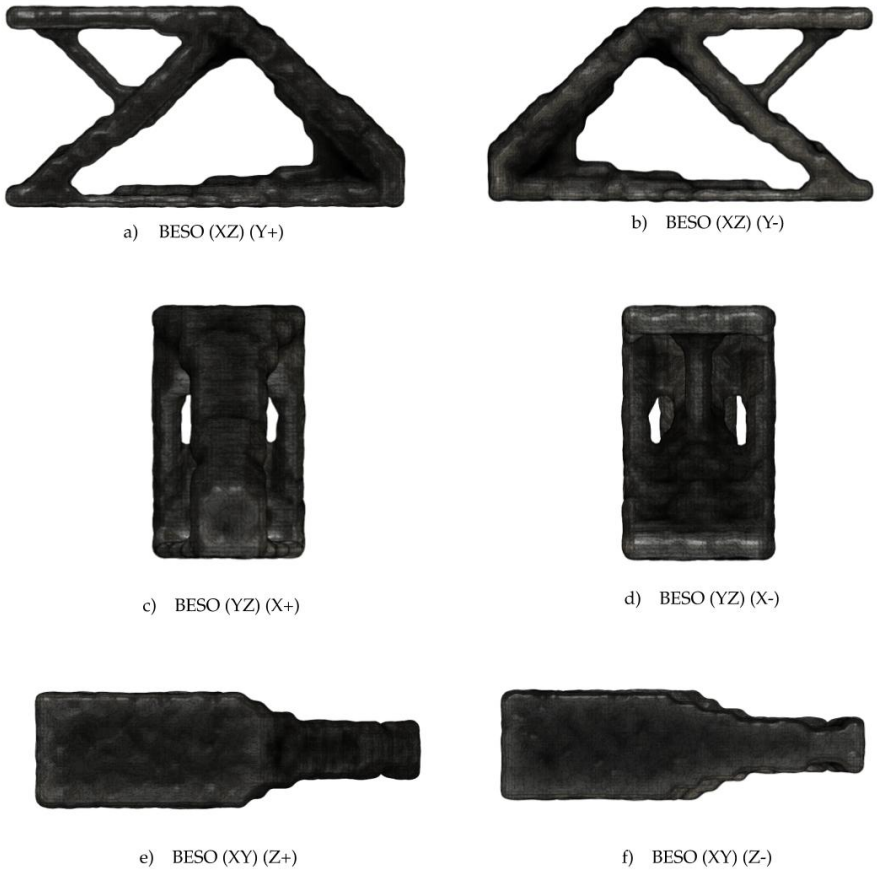

Figure B.4: 25% VF SIMP Cantilever with PSR Filter

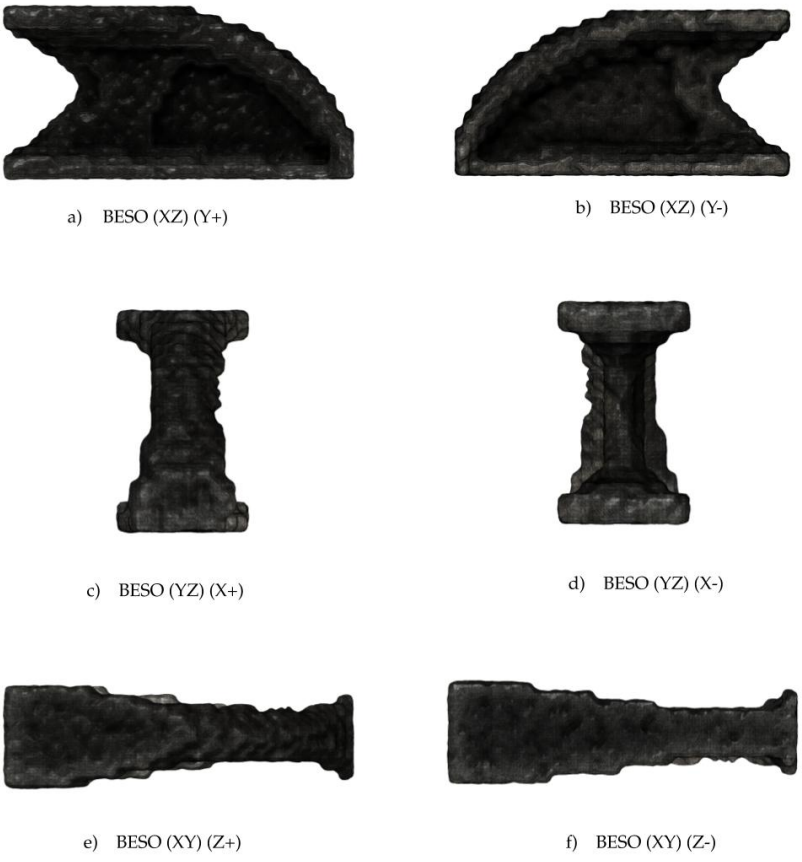

Figure B.5: 35% VF BESO Cantilever with PSR Filter

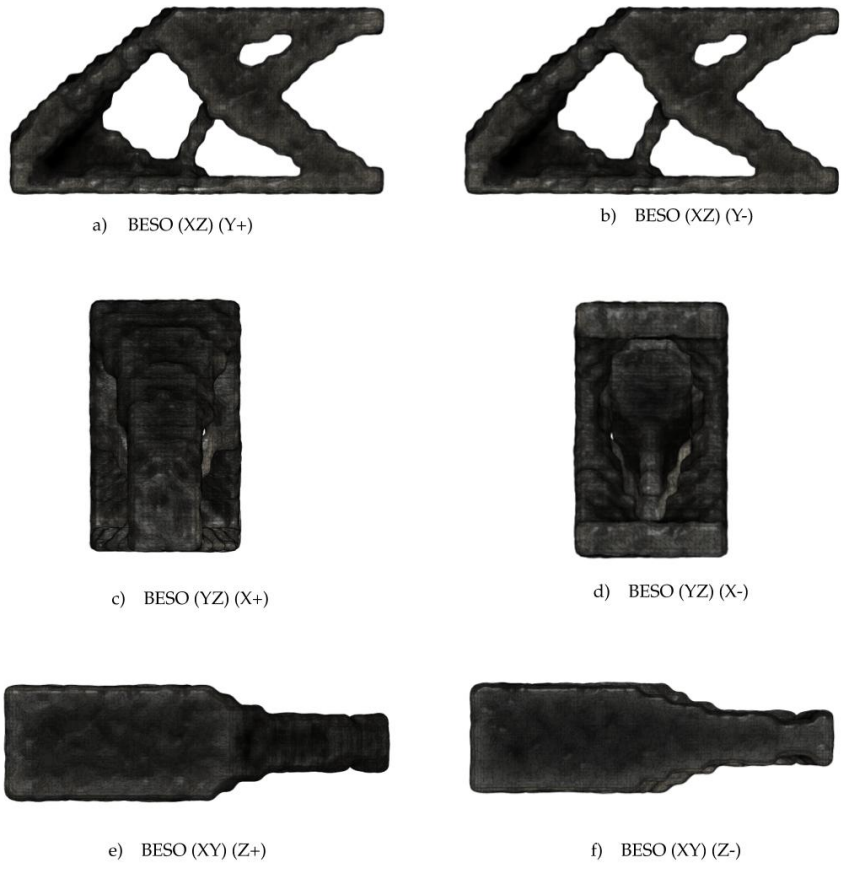

Figure B.6: 35% VF SIMP Cantilever with PSR Filter

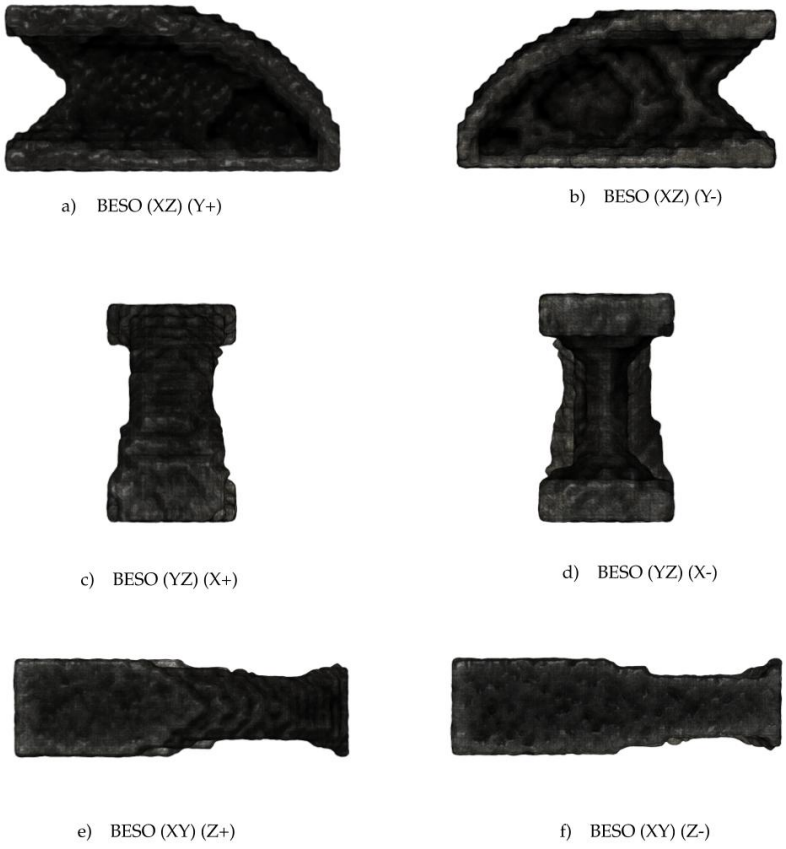

Figure B.7: 45% VF BESO Cantilever with PSR Filter

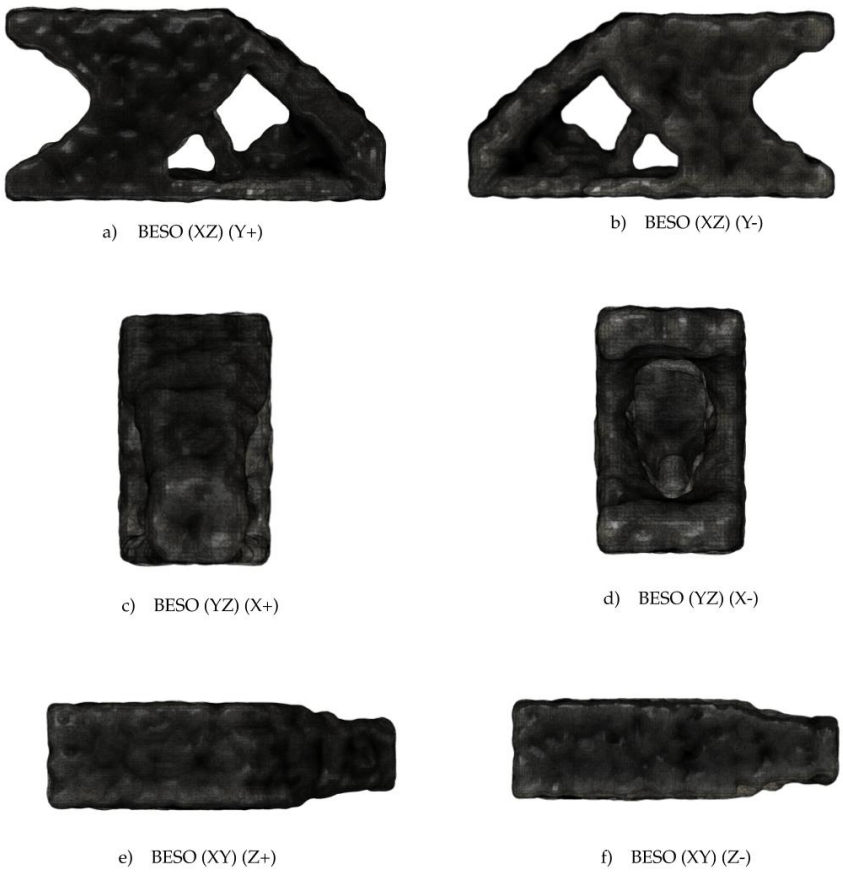

Figure B.8: 45% VF SIMP Cantilever with PSR Filter

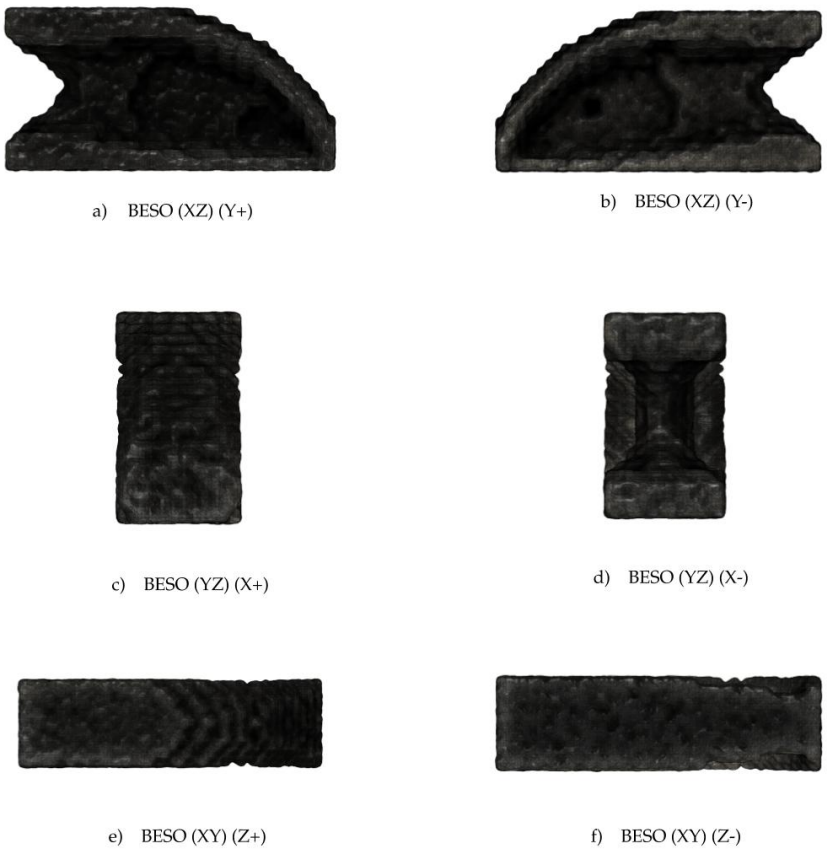

Figure B.9: 55% VF BESO Cantilever with PSR Filter

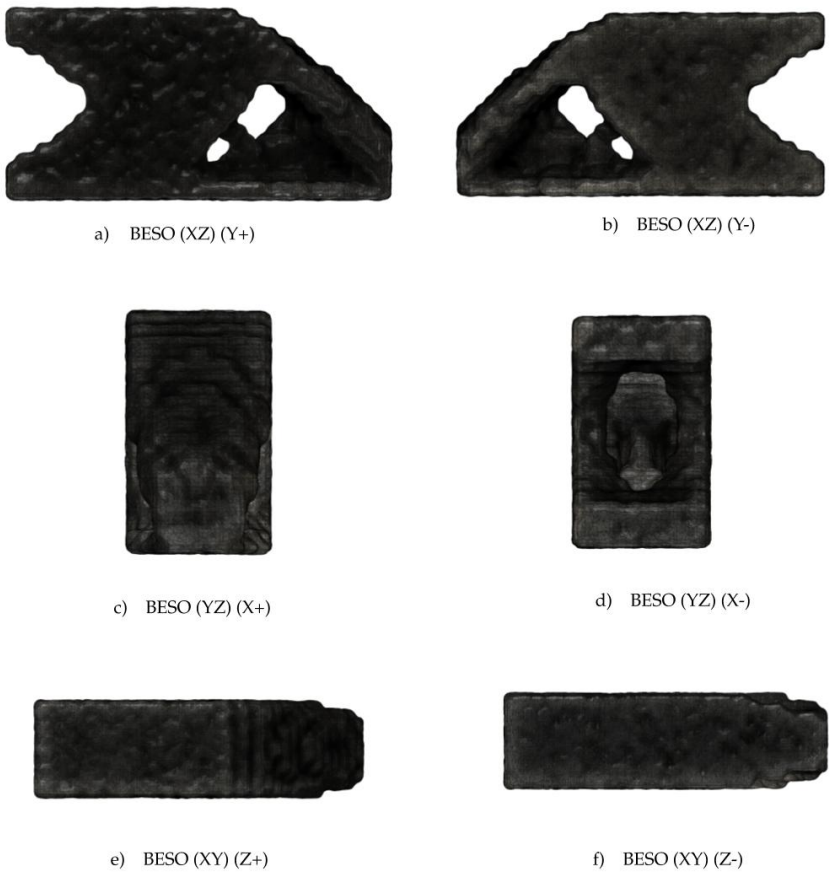

Figure B.10: 55% VF SIMP Cantilever with PSR Filter